

## Article

# Genesis of the Large-Scale Kamado Magnesite Deposit on the Tibetan Plateau

Xuhui Yu <sup>1,2,3</sup>, Guyue Hu <sup>2,\*</sup>, Yuchuan Chen <sup>2</sup>, Ying Xu <sup>4</sup>, Han Chen <sup>5</sup>, Denghong Wang <sup>2</sup>, Fan Huang <sup>2</sup>, Shuisheng You <sup>3</sup>, Haiyong Liu <sup>6</sup>, Liang He <sup>1,7</sup> and Yubin Li <sup>8</sup>

<sup>1</sup> College of Earth Sciences, Chengdu University of Technology, Chengdu 610059, China

<sup>2</sup> MNR Key Laboratory of Metallogeny and Mineral Assessment, Institute of Mineral Resources, Chinese Academy of Geological Sciences, Beijing 100037, China

<sup>3</sup> Sichuan Geology and Mineral Bureau Regional Geological Survey Team, Chengdu 610213, China

<sup>4</sup> Institute of Multipurpose Utilization of Mineral Resources, Chinese Academy of Geological Sciences, Chengdu 610041, China

<sup>5</sup> Sichuan Earthquake Administration, Chengdu 610041, China

<sup>6</sup> Geological Survey of Tibet Autonomous Region, Lhasa 850000, China

<sup>7</sup> No. 6 Geological Team, Tibet Bureau of Geology and Mineral Exploration and Development, Lhasa 851400, China

<sup>8</sup> College of Engineering, Tibet University, Lhasa 850000, China

\* Correspondence: wanghuguyue@126.com

**Abstract:** Lacustrine strata-bound magnesite deposits associated with Alpine-type ultramafic rocks are hydrothermal in origin. The magnesite ores of the Kamado deposit are unconformably underlain by mid-Jurassic marine carbonate and ultramafic rocks of the Bangong-Nujiang ophiolite suite and are in fault contact with hanging wall rocks composed of siliceous sinter. Three types of cryptocrystalline magnesite ores can be identified in Kamado: (1) strata-bound massive magnesites, representing the main ore type in the upper part; (2) banded ores in the lower part; and (3) some vein and stockwork ore in the ultramafic wall rocks. Integrated scanning electron microscopy, C–O isotope analysis, and geochemical analyses were carried out on the Kamado deposit. The results indicate that: (1) the orebody is composed of magnesite, with accessory minerals of aragonite, opal, and chromite; (2) the siliceous sinter and relatively high B (32.0–68.1 ppm) and Li (14.7–23.4 ppm) contents of the magnesite ores reflect long-term spring activity in Kamado; (3) the light carbon ( $\delta^{13}\text{C}_{\text{V-PDB}}$ :  $-4.7 \pm 0.3\%$  to  $-4.1 \pm 0.6\%$ ) and oxygen isotopic compositions ( $\delta^{18}\text{O}_{\text{V-SMOW}}$ :  $+12.3 \pm 0.3$  to  $+16.3 \pm 0.1\%$ ) of the stockwork ores in the foot wall rocks indicated that the carbon in fractures in the ultramafic rocks is from a mixture of marine carbonate and oxidized organic-rich sedimentary rocks, reflecting a typical “Kraubath-type” magnesite deposit; and (4) the relatively heavy carbon isotopic ( $\delta^{13}\text{C}_{\text{V-PDB}}$ :  $+8.7 \pm 0.4\%$  to  $+8.8 \pm 0.3\%$ ) composition of the banded magnesite ores in the lower segment may have formed from heavy  $\text{CO}_2$  generated by anaerobic fermentation in the lakebed. Additionally, the carbon isotopic ( $\delta^{13}\text{C}_{\text{V-PDB}}$ :  $+7.3 \pm 0.3\%$  to  $+7.7 \pm 0.7\%$ ) composition of the massive magnesite ores in the upper segment indicates a decline in the participation of anaerobic fermentation. As this economically valuable deposit is of the strata-bound massive ore type, Kamado can be classified as a lacustrine hydrothermal-sedimentary magnesite deposit, formed by continuous spring activities under salt lakes on the Tibetan Plateau, with the Mg mainly being contributed by nearby ultramafic rocks and the carbon mainly being sourced from atmosphere-lake water exchange, with minor amounts from marine carbonate strata.

**Keywords:** lacustrine hydrothermal-sedimentary mineralization; ultramafic rocks; suture zone; geochemistry; carbon isotopes; oxygen isotopes



**Citation:** Yu, X.; Hu, G.; Chen, Y.; Xu, Y.; Chen, H.; Wang, D.; Huang, F.; You, S.; Liu, H.; He, L.; et al. Genesis of the Large-Scale Kamado Magnesite Deposit on the Tibetan Plateau. *Minerals* **2024**, *14*, 45. <https://doi.org/10.3390/min14010045>

Academic Editor: Giorgio Garuti

Received: 19 October 2023

Revised: 27 December 2023

Accepted: 27 December 2023

Published: 29 December 2023



**Copyright:** © 2023 by the authors. Licensee MDPI, Basel, Switzerland. This article is an open access article distributed under the terms and conditions of the Creative Commons Attribution (CC BY) license (<https://creativecommons.org/licenses/by/4.0/>).

## 1. Introduction

Magnesite is one of the best raw materials for refractory industries and occurs in a wide variety of marine and nonmarine geological settings [1]. After a century of research,

the magnesium in (hydro) magnesite deposits has been considered to originate from (1) seawater [2–8], (2) Mg-rich precursor carbonates in and outside magnesite occurrences [9–11], or (3) the transformation and weathering of ultramafic complexes [12–18]. The traditional classifications of magnesite deposits are “Veitsch type” and “Kraubath type” after localities in Austria and Slovakia [2,19]. The magnesium in “Veitsch-type” magnesite deposits is sourced from (1) seawater or (2) Mg-rich precursor carbonates in and outside magnesite occurrences, and these deposits are characterized by sugary to coarse-grained spar forming nearly monomineralic lenses within marine platform sediments. In contrast, the magnesium in Kraubath-type deposits is sourced from (3) ultramafic complexes consisting of veins and stockworks of cryptocrystalline (bone-like) magnesite hosted by dunite and peridotite. Although this classification covers most magnesite deposits worldwide, there are still a few cryptocrystalline (or fine-grained) and lacustrine-origin magnesite deposits that do not fit easily within this classification scheme [20–23], such as the Barton Farm (Zimbabwe), Bela Stena (Serbia), and Hirsizdere (Turkey) deposits. As the magnesium in these lacustrine deposits is mainly sourced from the transformation or weathering of nearby ultramafic rock, Fallick et al. (1991) [24], Russell (1996) [25], Zedef et al. (2000) [26], and Schroll (2002) [27] suggested that these magnesite deposits could be classified in the “magnesites ultramafic associated group” and classified as the hydrothermal-sedimentary type. Furthermore, magnesites within ultramafic rocks can be formed in two conditions: (1) near surface epithermal systems with relatively low temperatures of 14–100 °C, which exhibit pure cryptocrystalline magnesite [28,29]; (2) during ophiolite emplacement or metamorphism at relatively high temperatures (>200 °C) [30,31], which exhibit dolomite and magnesite in talc-carbonate veins. Hydrothermal-sedimentary-type magnesite deposits are generally considered to have an evaporitic genesis with magnesium supplied by epithermal systems from nearby ultramafic rocks [24,26]. As rarely discovered worldwide, this metallogenic model of hydrothermal-sedimentary type magnesite deposit needs more specific examples to test.

The Kamado deposit is located in the eastern part of the Tethys tectonic belt, in Riwoche County of the Tibetan Autonomous Region, People’s Republic of China. The Kamado magnesite deposit, with ore reserves of 57.09 Mt and MgO grades above 47%, is the largest ultramafic-associated magnesite deposit in China [32,33]. The genesis of this deposit was attributed to the surface chemical weathering of ultramafic rocks [34,35], similar to the Attunga magnesite deposit in the New England Orogen, New South Wales, Australia [15–17]. However, during our field geological survey, we found that the outcrops of the Kamado magnesite ores were strata-bound and covered by siliceous sinter, which indicated that this deposit might have formed in relation to hydrothermal activity and not due to chemical weathering. Hydrothermal-sedimentary-type magnesite deposits have been reported in the western Tethyan region [24–26,36]. As the Mesozoic Bangong-Nujiang suture in southern Tibet can be compared to the ophiolites in Turkey and Serbia, this paper compares the geology, geochemistry, and C-O isotope data of the Kamado deposit to those of the lacustrine hydrothermal sedimentary magnesite deposits in the western Tethyan region (e.g., Bela Stena and Hirsizdere) and aims to constrain the genesis of the Kamado magnesite deposit in the Bangong-Nujiang suture zone and to establish a fundamental theory for magnesite deposit exploration in the suture zones of the eastern Tethyan region.

## 2. Geological Setting

### 2.1. Regional Geology

After the closure of the Tethyan ocean and Cimmeride blocks that accreted into the Euro-Asian continental margins, many supra-subduction zone (SSZ) Tethyan ophiolite suites formed in the region stretching from Southeast Asia and the Indo-Burma Mountains to the Tibetan and Iranian Plateaus to the Mediterranean Sea [37–39] (Figure 1). The Bangong-Nujiang suture zone (BNS), which contains one of the SSZ Tethyan ophiolites, is located in the eastern segment (Figure 1), extends for more than 2500 km across south-central Tibet, and separates the Lhasa Terrane in the south from the Qiangtang Terrane

in the north [40]. Well-preserved ophiolite complexes occur discontinuously in the BNS and are named the Ritu, Gaize, Dongco, Dongqiao, Amdo, and Dengqen complexes [41,42]. The Kamado magnesite deposit is associated with the Dengqen ophiolite complex, while the Dujiali hydromagnesite deposit is formed in the southwestern Palaeogene Lunpola graben basin, near the Dongqiao ophiolite complex (Figure 2).

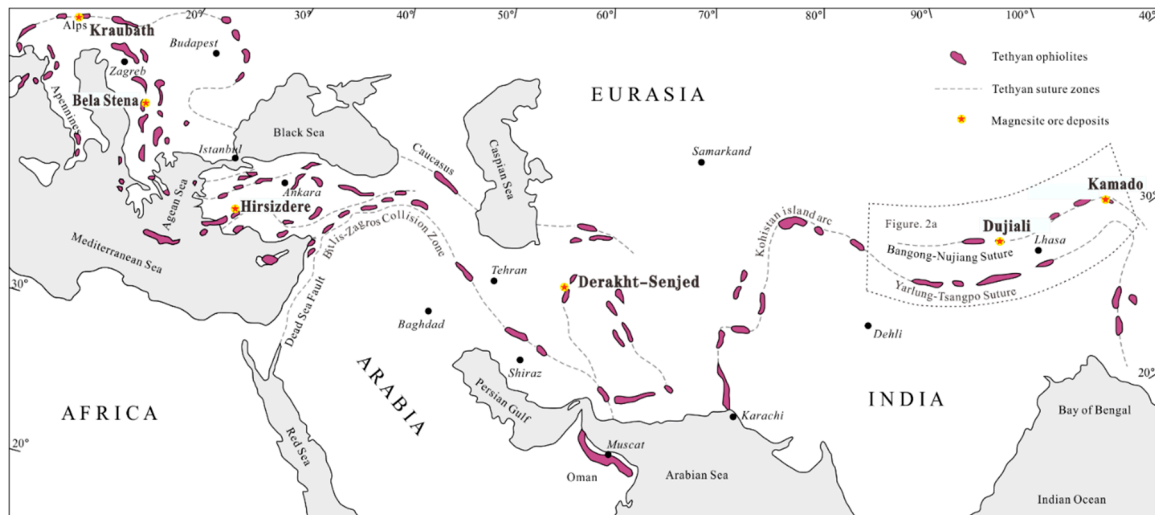


**Figure 1.** Distribution of lacustrine strata-bound magnesite deposits in the Alpine–Himalayan orogenic system (modified from [37]).

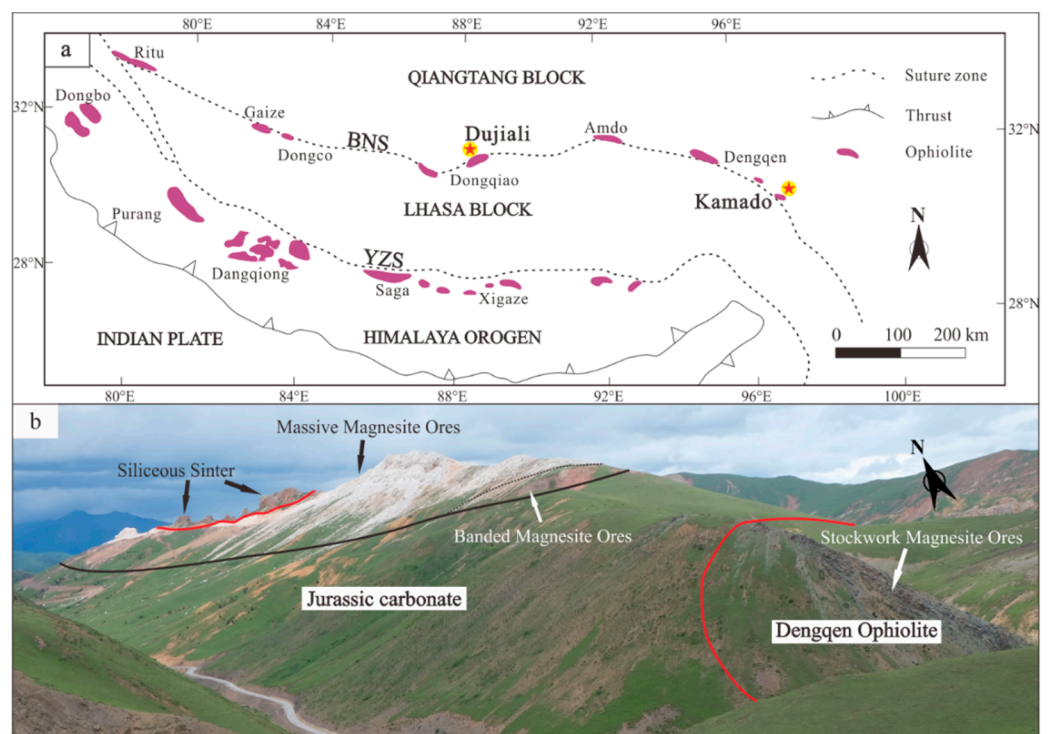


**Figure 2.** Tectonic and ophiolite distribution map of the study area (a) (modified from [41]) and remote view of sampling location in Kamado deposit (b). Abbreviations: BNS—Bangong–Nujiang Suture; YZS—Yarlung Zangbo Suture.

The India–Asia collision in the early Palaeogene and the subsequent continental deformation are thought to have caused the Tibetan Plateau to extrude towards the oceanic free boundary [43] and resulted in the development of a series of foreland basins within and

on the periphery of the Tibetan orogen [40]. The magmatic and sedimentary rocks of the Tibetan Plateau, especially the Miocene volcanic rocks in the Lhasa terrane, are enriched in B, Li, Rb, and Cs [44,45]. Since the related strike-slip and normal faults are linked to hot crustal anatectic magmas at depth, the upwelling of high-temperature water may affect the supply of B, Li, Rb, and Cs to salt lakes [46,47]. Similar to the hydrothermal-sedimentary (hydro)magnesite deposits in Serbia [24] and Turkey [26], a few (hydro)magnesite deposits (e.g., Kamado and Dujiali) have been recognized in the BNS.

## 2.2. Geology of the Kamado Magnesite Deposit

The Kamado magnesite deposit is located in the eastern segment (Dengqen ophiolite) of the BNS [41,48] inside the dextral strike-slip geological complex of eastern Tibet (Figure 2). Because of the closure of the Bangong-Nujiang Ocean and the emplacement of the Dengqen ophiolite in the Late Jurassic–Early Cretaceous [49], most of the geological bodies in the Kamado mining area are in fault contact with each other. The Cenozoic strata-bound magnesite orebody occurs below geothermal siliceous sinter and unconformably overlies the Dengqen ophiolite complex, which includes Mesozoic Alpine-type ultramafic rocks and Jurassic carbonate rocks (Figure 3a,b). The Kamado magnesite orebody is strata-bound, with a length of approximately 1800 m, a width of 100–150 m, and a thickness of 60–80 m in the mining area. It is in unconformable contact with footwall rocks composed of Middle Jurassic dolomites and in fault contact with hanging wall rocks composed of siliceous sinter (Figure 4a). Three types of magnesite ores have been identified in the Kamado deposit, including, from bottom to top, (1) stockwork or vein ores in ultramafic rocks and carbonates (Figure 4b), (2) banded ores (Figure 4c), and (3) massive ores (Figure 4a).

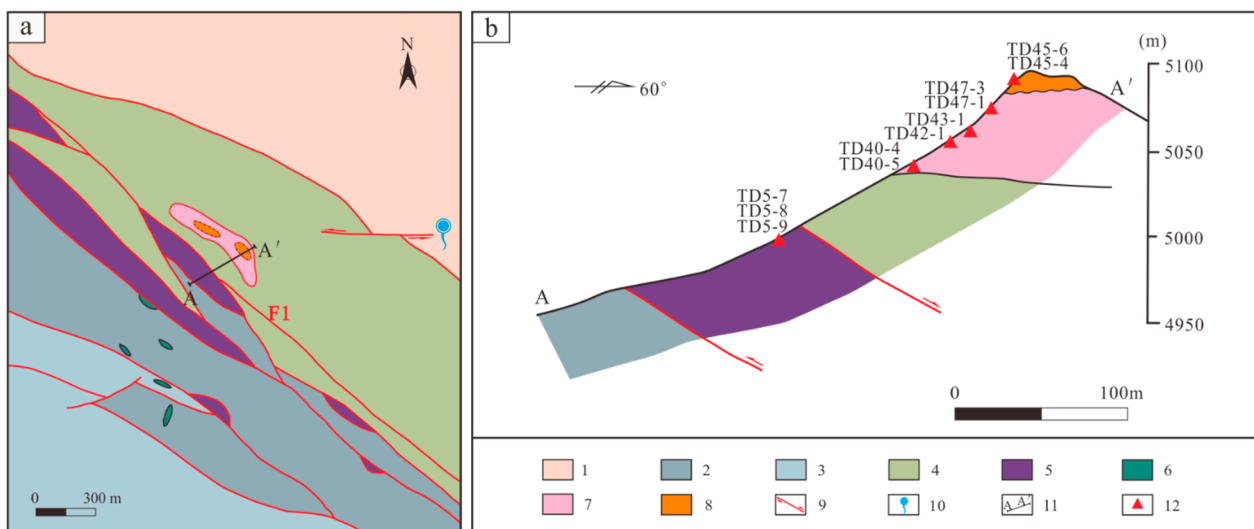


**Figure 3.** Geological map (a) and sampling profile (b) of the Kamado magnesite. 1—Middle part of Sangduo Formation, Upper Triassic; 2—First part of Luodong Group, Lower Jurassic; 3—Fourth part of Luodong Group, Lower Jurassic; 4—The first part of Yanshiping Group, Middle Jurassic; 5—Dingqing ophiolite; 6—Diabasic dike; 7—Orebody of magnesite; 8—Siliceous sinter; 9—Fault and movement direction; 10—Modern warm spring; 11—Position of section line; 12—Sampling location.

The vein or stockwork magnesite ores crop out in the footwall rocks of ultramafic rocks in the Dengqen ophiolite (Figure 2b). These vein or stockwork ores are commonly developed from harzburgites, which can be classified as the Kraubath type [28] and are considered to have formed in the early stage of mineralization. The banded magnesite ores distributed on the floor ore body or sedimentary unconformities (Figure 2b) are formed in the middle stage and have a light grey, cryptocrystalline texture. Massive ores are the main body and conformable contact above banded ores and are the most economically valuable ores mined in the Kamado deposit. They are formed in the late stages and are similar to

the magnesite ores of the Bela Stena deposit [24]. They are usually white, rarely light red, and mainly characterized by a cryptocrystalline texture, soil lustre, conchoidal fracture surface, a hardness of approximately 5 (Mohs Hardness Scale), and a particle size less than 4  $\mu\text{m}$ . The gangue minerals of the deposit are small amounts of dolomite (Figure 5d,e), aragonite (Figures 4d and 5a), and opal (Figures 4e and 5a), with overall contents of less than 2%. Based on the field characteristics, the vein or stockwork ores may be the product of hydrothermal metamorphism, and the banded ores and the massive ores are the result of sedimentation.

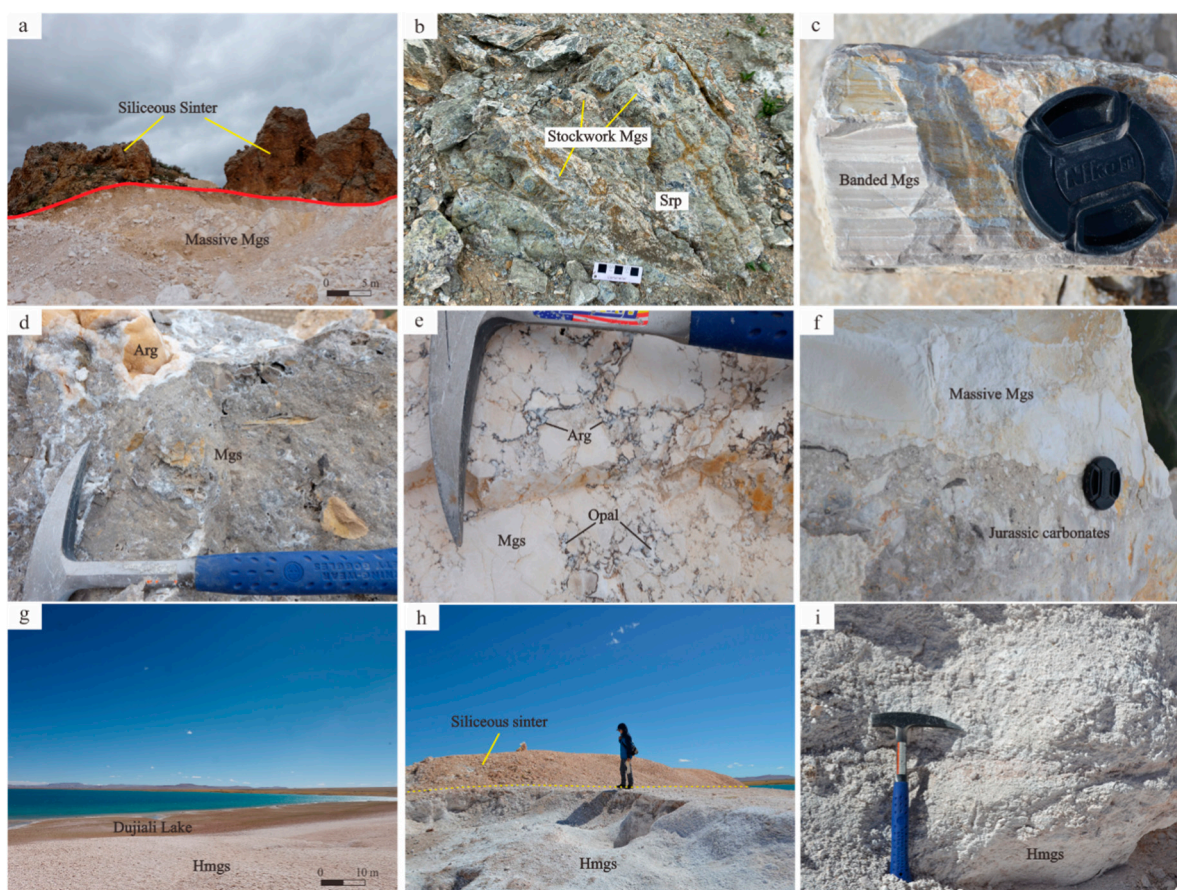


**Figure 4.** Photographs of typical magnesite ores from the Kamado deposit: (a) The massive magnesite orebody in fault contact with siliceous sinter, (b) stockwork magnesite in ultramafic rocks, (c) banded magnesite ore, (d,e) aragonite in cracks in cryptocrystalline magnesite, (f) the magnesite ore body unconformably overlies Jurassic carbonate strata, (g) hydromagnesite on the shore of Dujiali Lake, (h) siliceous sinter on the top of hydromagnesite, and (i) hydromagnesite with earthy lustre. Abbreviations: Mgs—Magnesite; Srp—Serpentine; Arg—Aragonite; Hmgs—Hydromagnesite.

### 2.3. Hydromagnesite in Lake Dujiali

Dujiali Lake is located in the central Tibetan Plateau (Figures 1 and 2a). It is a semi-closed endorheic basin that is mainly recharged by meteoric water and groundwater. And it is one of the few salt lakes in the world that extensively deposits hydromagnesite. [7,50].

Structurally, the lake is located at the centre of the Banggong-Nujiang suture zone within the Lampora Paleogene faulted basin. Hydromagnesite is directly deposited on the Holocene sediments (Figure 4g), with a layer of yellow-brown, hard siliceous sinter on the surface (Figure 4h) that is mixed with Holocene mud and sand. After removing the weathered crust, it becomes a snow-white block of hydromagnesite with an earthy lustre (Figure 4i).

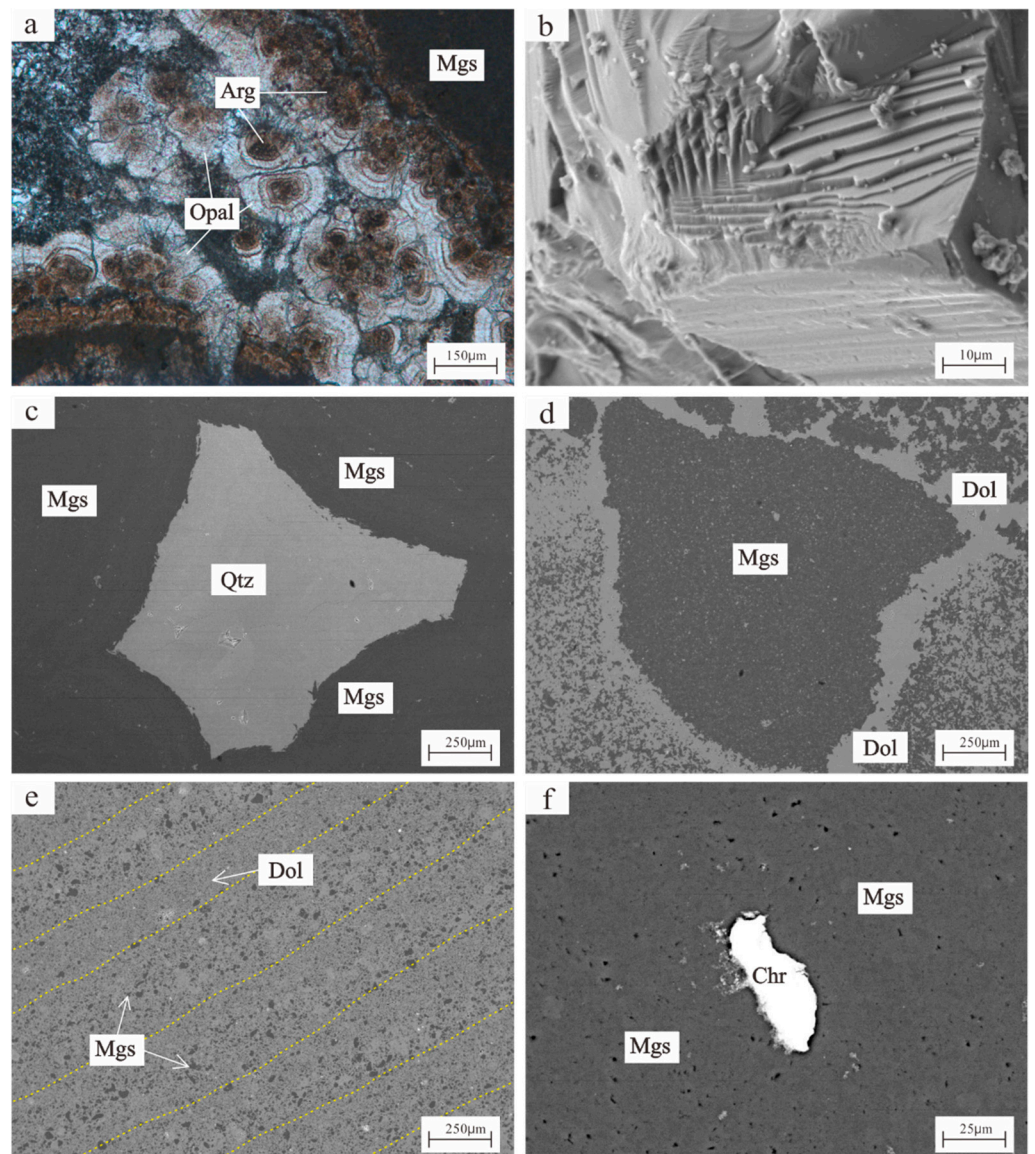


**Figure 5.** Microscopic photos and BSE images of the fabric characteristics of magnesite ore from the Kamado deposit: (a) Opal formed at low temperatures in cryptocrystalline magnesite; (b) stepped growth lines can be observed under the natural fracture surface that are enlarged by 1150 times; (c) magnesite crystallized along the edge of quartz brings about a zonal texture; (d) dolomite is often metasomatized by cryptocrystalline magnesite in irregular or diffuse shapes; (e) dolomite debris redeposited with cryptocrystalline magnesite to form banded magnesite ore; (f) allomorphic magnesiochromite appears in banded cryptocrystalline magnesite occasionally. Abbreviations: Mgs—Magnesite; Arg—Aragonite; Qtz—Quartz; Dol—Dolomite; Chr—Chromite.

### 3. Sampling and Analytical Methods

This study selected a total of 16 representative samples in three types, including 12 magnesite ores, 2 dolomites, and 2 siliceous sinters from the Kamado magnesite deposit. A magnesite ore sample is the key object of this paper. The sample includes 7 massive magnesite ores, 2 banded magnesite ores, and 3 stockwork magnesite ores. The morphology and texture of magnesite ore and its relationship with hydrothermal minerals were observed by an optical microscope and a scanning electron microscope. The main chemical composition, trace elements, and carbon and oxygen isotope composition of Kamado magnesite ores were obtained by whole-rock geochemistry analysis and carbon and oxygen isotope analysis, making them convenient for comparative study with other deposits.

### 3.1. Scanning Electron Microscopy (SEM)

Scanning electron microscopy and micro-area energy spectrum tests were completed at the Laboratory of Rock and Process Mineralogy, Institute of Comprehensive Utilization of Mineral Resources, Chinese Academy of Geological Sciences. The polished samples were sprayed with carbon on the surface and placed into a scanning electron microscope (Sigma300, Carl Zeiss, Germany) sample bin equipped with a energy spectrometer (XFlash 6160, Bruker, Germany). Under the conditions of a high voltage of 20 kV and a working distance of WD = 10.1 mm, backscatter images of the target mineral were observed and collected, and an energy spectrometer was used to collect the characteristic X-ray energy spectrum of the target mineral micro-area to obtain the element composition and relative content of the micro-area.

### 3.2. Whole-Rock Geochemistry Analysis

Whole-rock powders for magnesites, dolomites, and ultrabasic rocks were prepared by using a tungsten carbide shatter box. Bulk rock major and boron concentrations were obtained by X-ray fluorescence spectrometer (Axios Pw4400, PANalytical B.V., Almelo, The Netherlands) and inductively coupled plasma–mass spectrometry (PE300Q, PerkinElmer, Waltham, MA, USA.) at the National Research Center for Geoanalysis, CAGS, Beijing. Major elements were analysed by the XRF method with analytical uncertainties of <5%. Lithium and boron concentrations were analysed by ICP-MS. Analytical uncertainties were 10% for elements with abundances of <10 ppm and approximately 5% for those with abundances of >10 ppm. The analytical results are listed in Table 1.

**Table 1.** Composition of major and trace element data for the ores and host rocks of Kamado magnesite deposits.

Sample No.	TD20-40-4	TD20-40-5	TD20-42-1	TD20-43-1	TD20-47-1	TD20-47-2	TD20-47-3	TD20-48-1	TD20-45-8	TD20-45-11	TD20-45-4	TD20-45-6
Rock Type	Banded Magnesite		Massive Magnesite						Dolomite		Siliceous Sinter	
SiO <sub>2</sub> (%)	5.40	3.50	<0.01	<0.01	0.76	<0.01	0.13	1.10	5.12	3.31	98.91	98.80
Al <sub>2</sub> O <sub>3</sub> (%)	0.85	0.66	0.04	0.05	0.05	0.05	0.05	0.30	0.12	0.12	0.74	0.96
CaO (%)	2.98	4.32	0.59	1.73	1.06	0.66	0.57	0.95	18.90	17.84	0.17	0.15
TFe <sub>2</sub> O <sub>3</sub> (%)	0.53	0.44	0.03	0.03	0.05	0.02	0.04	0.04	0.17	0.13	0.09	0.07
FeO (%)	0.32	0.28	<0.01	<0.01	0.04	<0.01	0.04	0.04	0.07	0.11	0.05	0.05
K <sub>2</sub> O (%)	0.12	0.21	0.02	0.02	0.02	0.02	0.02	0.04	0.02	<0.01	0.03	0.03
MgO (%)	42.19	43.55	48.53	47.32	47.37	48.33	48.03	47.00	30.07	33.27	0.19	0.11
MnO (%)	0.01	0.02	<0.01	<0.01	<0.01	<0.01	<0.01	<0.01	0.01	0.06	<0.01	<0.01
Na <sub>2</sub> O (%)	0.07	0.12	0.07	0.10	0.09	0.09	0.07	0.09	0.02	0.01	<0.01	<0.01
P <sub>2</sub> O <sub>5</sub> (%)	0.42	0.35	<0.01	<0.01	<0.01	<0.01	<0.01	<0.01	<0.01	<0.01	<0.01	<0.01
TiO <sub>2</sub> (%)	0.06	0.05	0.03	0.02	0.02	0.02	0.02	0.03	0.02	<0.01	0.02	0.01
CO <sub>2</sub> (%)	45.48	44.36	49.19	49.19	49.67	50.64	50.46	50.24	44.20	44.62	0.34	0.34
H <sub>2</sub> O <sup>+</sup> (%)	0.90	1.10	1.14	0.42	0.70	0.32	0.70	0.26	1.12	1.06	0.36	0.14
LOI (%)	46.72	45.88	50.82	50.35	50.61	51.30	51.13	50.76	45.13	45.84	0.49	0.48
Total	99.67	99.38	100.13	99.62	100.07	100.49	100.1	100.35	99.65	100.69	100.69	100.66
B (ppm)	24.5	23.4	32.0	68.1	52.5	52.9	42.4	50.0	<2.00	<2.00	2.66	12.4
Li (ppm)	13.5	15.2	14.7	23.4	20.1	21.1	18.5	20.4	4.41	3.19	52.4	87.3
La (ppm)	1.85	1.32	<0.05	<0.05	<0.05	<0.05	<0.05	<0.05	0.07	0.13	0.23	0.23
Ce (ppm)	4.00	3.25	0.09	0.10	0.07	<0.05	<0.05	<0.05	0.15	0.28	0.40	0.39
Pr (ppm)	0.42	0.30	<0.05	<0.05	<0.05	<0.05	<0.05	<0.05	<0.05	<0.05	<0.05	<0.05
Nd (ppm)	1.39	0.82	<0.05	<0.05	<0.05	<0.05	<0.05	<0.05	0.10	0.16	0.13	0.13
Sm (ppm)	0.23	0.26	<0.05	<0.05	<0.05	<0.05	<0.05	<0.05	<0.05	0.06	<0.05	<0.05
Eu (ppm)	<0.05	<0.05	<0.05	<0.05	<0.05	<0.05	<0.05	<0.05	<0.05	<0.05	<0.05	<0.05
Gd (ppm)	0.22	0.15	<0.05	<0.05	<0.05	<0.05	<0.05	<0.05	0.11	0.12	<0.05	<0.05
Tb (ppm)	<0.05	<0.05	<0.05	<0.05	<0.05	<0.05	<0.05	<0.05	<0.05	<0.05	<0.05	<0.05
Dy (ppm)	0.20	0.22	<0.05	<0.05	<0.05	<0.05	<0.05	<0.05	0.09	0.10	<0.05	<0.05
Ho (ppm)	<0.05	<0.05	<0.05	<0.05	<0.05	<0.05	<0.05	<0.05	<0.05	<0.05	<0.05	<0.05
Er (ppm)	0.11	0.18	<0.05	<0.05	<0.05	<0.05	<0.05	<0.05	<0.05	<0.05	<0.05	<0.05
Tm (ppm)	<0.05	<0.05	<0.05	<0.05	<0.05	<0.05	<0.05	<0.05	<0.05	<0.05	<0.05	<0.05
Yb (ppm)	0.12	0.16	<0.05	<0.05	<0.05	<0.05	<0.05	<0.05	<0.05	<0.05	<0.05	<0.05
Lu (ppm)	<0.05	<0.05	<0.05	<0.05	<0.05	<0.05	<0.05	<0.05	<0.05	<0.05	<0.05	<0.05
Y (ppm)	1.12	0.92	0.10	0.12	0.11	0.10	0.06	<0.05	0.60	0.59	0.75	0.95

### 3.3. Carbon and Oxygen Isotope Analysis

The carbon and oxygen isotopic compositions of the Kamado magnesite deposit were analysed at the Institute of Mineral Resources, Chinese Academy of Geological

Sciences. The magnesites were flushed with helium in a headspace vial and then reacted with phosphoric acid at 70 °C for 24 h. Analyte CO<sub>2</sub> was measured for carbon and oxygen isotopes using a Gasbench II attached to a MAT 253 continuous flow-isotope ratio mass spectrometer. The analytical precision of carbon and oxygen isotopes was  $\pm 0.2\%$ . The method was first calibrated using four in-house calcite standards: GBW04405 ( $\delta^{13}\text{C}_{\text{V-PDB}} = 0.57\%$ ,  $\delta^{18}\text{O}_{\text{V-PDB}} = -8.49\%$ ), GBW04406 ( $\delta^{13}\text{C}_{\text{V-PDB}} = -10.85\%$ ,  $\delta^{18}\text{O}_{\text{V-PDB}} = -12.40\%$ ), GBW04416 ( $\delta^{13}\text{C}_{\text{V-PDB}} = 1.6\%$ ,  $\delta^{18}\text{O}_{\text{V-PDB}} = -11.59\%$ ), and GBW04417 ( $\delta^{13}\text{C}_{\text{V-PDB}} = -6.06\%$ ,  $\delta^{18}\text{O}_{\text{V-PDB}} = -24.12\%$ ). Afterwards, the oxygen isotope fractionation during the phosphoric acid digestion at 70 °C was corrected by applying the acid fractionation factor of 1.01008 for magnesite and 1.00871 for calcite [51,52]. The results were normalized by using V-PDB (Vienna Pee Dee Belemnite) and V-SMOW (Standard Mean Ocean Water) [53]. These results are listed in Table 2.

**Table 2.** Carbon and oxygen isotope data for the ores of Kamado magnesite deposits.

Sample No.	Sample Type	Mineralization Stage	$\delta^{13}\text{C}_{\text{V-PDB}}$ (‰)			$\delta^{18}\text{O}_{\text{V-PDB}}$ (‰)		$\delta^{18}\text{O}_{\text{V-SMOW}}$ (‰)		
			Single	Mean	2SD	Single	Mean	Single	Mean	2SD
TD22-5-7	Stockwork magnesite	Early stage	−4.5	−4.6	0.3	−18.0	−18.1	+12.4	+12.3	0.3
TD22-5-7'			−4.7			−18.2		+12.1		
TD22-5-8			−4.8			−17.6		+12.8		
TD22-5-8'			−4.6			−17.2		+13.2		
TD22-5-9			−3.9			−14.2		+16.3		
TD22-5-9'			−4.3			−14.1		+16.4		
TD20-40-4	Banded magnesite	Middle stage	+8.7	+8.8	0.3	−8.0	−7.7	+22.7	+23.0	1.0
TD20-40-4'			+8.9			−7.3		+23.4		
TD20-40-5			+8.5			−8.1		+22.6		
TD20-40-5'			+8.8			−7.6		+23.1		
TD20-42-1	Massive magnesite	Late stage	+7.2	+7.4	0.4	−2.5	−2.4	+28.3	+28.4	0.3
TD20-42-1'			+7.5			−2.3		+28.5		
TD20-43-1			+7.2			−2.5		+28.3		
TD20-43-1'			+7.4			−2.4		+28.4		
TD20-47-1			+7.4			−3.2		+27.6		
TD20-47-1'			+7.9			−2.9		+27.9		
TD20-47-3			+7.7			−3.8		+27.0		
TD20-47-3'			+7.7			−3.7		+27.1		
TD22-2-1			+7.5			−1.3		+29.6		
TD22-2-1'			+7.7			−1.5		+29.4		

Note: The  $\delta^{18}\text{O}$  value in the main body and figures of this paper are presented relative to V-SMOW [53]. The sample numbers with an apostrophe (') are the same samples from the repeated test. 2SD, 2 times the standard deviation.

## 4. Results

### 4.1. Scanning Electron Microscopy

The secondary electron image of the scanning electron microscope showed the cryptocrystalline structure of Kamado high-purity magnesite, and no other minerals were observed except for crystal residual holes at 800 times magnification (Figure 5c–e). Stepped growth lines are observed when the natural fracture surface is enlarged by 1150 times (Figure 5b). At the early stage of mineralization, cryptocrystalline magnesite crystallized along the edge of quartz in the ore-forming hydrothermal solution, forming a zonal texture (Figure 5c). In contact with surrounding rocks, the Middle Jurassic dolomite is often metasomatized by cryptocrystalline magnesite in irregular or diffuse shapes (Figure 5d). Some dolomite debris was redeposited with cryptocrystalline magnesite to form banded magnesite ore (Figure 5e). In addition, allomorphic chromite occasionally appears in the banded cryptocrystalline magnesite (Figure 5f).

### 4.2. Whole-Rock Geochemistry

The magnesite ores generally had a high MgO content, which ranged from 47.00% to 48.53%, and low contents of CaO and SiO<sub>2</sub>, which ranged from 0.59% to 1.73% and from <0.01% to 1.10%, respectively. An inverse correlation exists between magnesium and calcium content.

The dolomites of the floor wall rocks had contents of CaO (17.84–27.91%) and MgO (24.38–33.27%). The siliceous sinters on the top of the ore body had high SiO<sub>2</sub> contents above 98.00%, and the other components had a combined average value of only 1.82%.

The magnesite ores are obviously poor in rare earth elements; massive ore was lower than 0.22 ppm, except for banded magnesite, which reached 9.66 ppm but was enriched with a few trace elements, such as boron (24.5–68.1 ppm) and lithium (13.5–23.4 ppm). The content of lithium in siliceous sinter was relatively enriched, with an average of 69.9 ppm and a maximum of 87.3 ppm.

#### 4.3. Carbon and Oxygen Isotopes

The carbon and oxygen isotope compositions of one piece of stockwork magnesite ore, three pieces of detrital magnesite ores at the early stage of mineralization, one piece of banded magnesite ore at the middle stage of mineralization, and five pieces of massive magnesite ores at the late stage of mineralization were determined from the Kamado magnesite deposit. The  $\delta^{13}\text{C}_{\text{V-PDB}}$  and  $\delta^{18}\text{O}_{\text{V-SMOW}}$  values of stockwork magnesite ore were  $-4.7 \pm 0.3\text{‰}$  to  $-4.1 \pm 0.6\text{‰}$  and  $+12.3 \pm 0.3$  to  $+16.3 \pm 0.1\text{‰}$ , respectively. The banded magnesite ores analysed had  $\delta^{13}\text{C}_{\text{V-PDB}}$  values ranging from  $+8.7 \pm 0.4\text{‰}$  to  $+8.8 \pm 0.3\text{‰}$  and  $\delta^{18}\text{O}_{\text{V-SMOW}}$  values ranging from  $+22.8 \pm 0.7\text{‰}$  to  $+23.0 \pm 1.0\text{‰}$ . The massive magnesite ores had centralized  $\delta^{13}\text{C}_{\text{V-PDB}}$  values ranging from  $+7.3 \pm 0.3\text{‰}$  to  $+7.7 \pm 0.7\text{‰}$  and  $\delta^{18}\text{O}_{\text{V-SMOW}}$  values ranging from  $+27.1 \pm 0.4\text{‰}$  to  $+29.5 \pm 0.3\text{‰}$  (Figure 6).

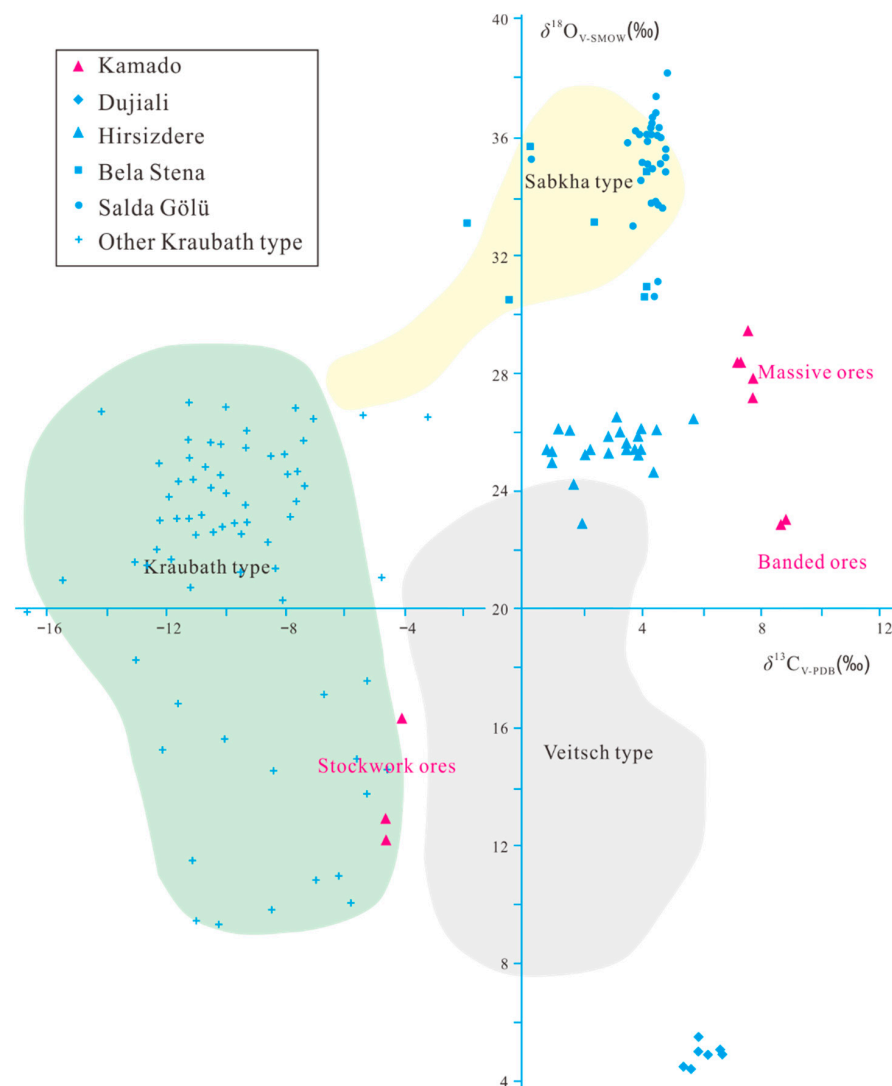


**Figure 6.** Plot of carbon and oxygen isotopic compositions of magnesites from the Kamado magnesite deposit together with cryptocrystalline magnesites in lacustrine hydrothermal sedimentary strata worldwide (genetic type of magnesite cited from [28]) showing the data of Bela Stena magnesite [24], Salda Gölü and Hirsizdere magnesite [26], Dujiali hydromagnesite [54], and other Kraubath types [28].

## 5. Discussion

### 5.1. Magnesium Sources of the Kamado Magnesite Deposit

Stockwork or vein magnesite ores can be identified in the floor wall rocks of the Dengqen ophiolite (Figures 2b and 4b), representing the epithermal routes and ore-hosting sites [28,55]. The occurrence of stockwork or vein magnesite ores in the Kamado is similar to that of the “Kraubath type observed” worldwide [13,28]. Regionally, research on inert gases in hot springs suggests that large strike-slip faults may reach deep into the mantle [56–58], and significant regional high-temperature hot spring activity is triggered by higher geothermal gradients [47,59,60]. In the mining area, the siliceous sinter was in fault contact with the hanging wall (Figure 2b), and a modern thermal spring still exists nearby (Figure 3a). Furthermore, the chemical composition of surface water around Dujiali Lake evolved from the rock-weathering-type waters of T1 (Ca-Mg-HCO<sub>3</sub> water type) to more concentrated sodic waters of T2 (Na-SO<sub>4</sub>-Cl water type) due to evaporation [54,61]. Therefore, the high-temperature circulating groundwater in Kamado may have had the ability to take much magnesium from ultrabasic or/and magnesium-rich carbonate rocks into the surface lakes [62]. In contrast, the exceedingly low REE contents of banded ores and massive ores may crystallize at lower temperatures [63,64], and aqueous solution conditions for plateau lakes with alkalinity (pH > 7) [65] support the obvious assumption that Mg<sup>2+</sup> is derived from ultramafics, which are poor in REEs [27,66,67].

The continuously upwelling magnesium-rich thermal water fed the evaporative lake and may have formed hydromagnesite-bearing sediments, similar to those in Dujiali Lake [54,61] or Salda Lake [26,68]. During the process of dissolving ultrabasic rock magnesium, hot springs may also bring a small amount of dissolved silica into the lake. Consequently, large amounts of opal were formed in the ores (Figure 5a), and small amounts of chromite and other minerals were transported from ultrabasic rocks that formed synsedimentary deposits in magnesite ore bodies (Figure 5f). The residual silica formed siliceous sinters above or around the magnesite ore body (Figure 4a,h), and significant trace elements such as B and Li were preserved in the siliceous sinters and magnesite ores (Table 1). Additionally, the calcium content in the dissolved Middle-Jurassic carbonate strata increased, forming a small amount of aragonite in the ore body (Figure 4e). Compared to quartz, the distribution of aragonite in banded and massive magnesite ores was extremely limited, indicating that the magnesium in the Kamado deposit was mainly sourced from ultramafic rocks, with minor amounts from marine carbonate strata.

### 5.2. Carbon Sources of the Kamado Magnesite Deposit

The oxygen isotope analysis of the hydromagnesite indicates that supergene formation with authigenic carbonate crystallization from evaporation water is the dominant precipitation process. Combined carbon–oxygen isotope analysis suggests that atmospheric CO<sub>2</sub> provided a carbon source for the precipitation of hydromagnesite. These findings suggest that hydromagnesite precipitation at Lake Dujiali is mainly inorganic in nature, and the greenhouse gas, CO<sub>2</sub>, is trapped and stored in the hydromagnesite directly from the atmosphere [54,61]. The carbon isotope composition ( $\delta^{13}\text{C}_{\text{V-PDB}} = -4.7 \pm 0.3\text{‰}$  to  $-4.1 \pm 0.6\text{‰}$ ) of the vein or stockwork magnesite ores in Kamado fell within the carbon isotope range of the Kraubath type ( $-20$  to  $-4\text{‰}$ ) but was higher than the peak value ( $-12$  to  $-9\text{‰}$ ) [20]. The carbon sources for Kraubath-type magnesite deposits include volcanoes, residual gas in soil, marine carbonate, or organic carbon ([69] and the references therein). As there has been no volcanic activity in the area since the Cenozoic era and the collection of vein-like ores is in the ultrabasic rocks below the main ore body, the carbon sources for stockwork magnesite ore are best explained by a mixture of oxidized organic carbon and dissolved marine carbonates. The  $\delta^{13}\text{C}_{\text{V-PDB}}$  values of organic matter are generally below  $-10\text{‰}$ , while the value is approximately zero for marine carbonate [70]. Therefore, the carbon contribution of carbonate may have exceeded 50% during the mixing process. The oxygen isotope values of the stockwork ore also support the argument that the anion sources of the Kamado stockwork ore may be slightly different from those of most Kraubath-type magne-

site ores. The  $\delta^{18}\text{O}_{\text{V-SMOW}}$  value ranged from  $+12.3 \pm 0.3\%$  to  $+16.3 \pm 0.1\%$ , which was significantly lower than that of the Kraubath type ( $+22$  to  $+29\%$ ) [20]. The clumped-isotope thermometry study of Kraubath-type magnesite deposits suggests that the worldwide cryptocrystalline magnesite ores were formed at a temperature of  $23\text{--}28\text{ }^\circ\text{C}$  [29]. Most of the researchers estimated that the temperature of formation of cryptocrystalline magnesite in various deposits worldwide varies from  $\sim 14$  to  $100\text{ }^\circ\text{C}$  [24,26,71]. As formed at relatively low temperatures, the relative lower values of  $\delta^{18}\text{O}_{\text{V-SMOW}}$  in this study may result from meteoric oxygen isotopic fractionation at the high altitude of the Tibet Plateau.

The carbon isotope composition ( $\delta^{13}\text{C}_{\text{V-PDB}} = +8.7 \pm 0.4\%$  to  $+8.8 \pm 0.3\%$ ) of the banded magnesite ore shows an extremely positive anomaly. This extremely  $\delta^{13}\text{C}$  positive anomaly data can also be seen in 2.33–2.06 Ga marine carbonate formation [72–74], which can be high to  $+13.4\%$  in dolomites of the Lomagundi Group [75] and be termed the Lomagundi event [76]. The giant magnesite deposits in the Liaodong peninsula are hosted in the Paleoproterozoic Liaohe Group and show a positive  $\delta^{13}\text{C}$  anomaly [77]. Billions of years ago, deep under the ocean, the pores and pockets in minerals that surround warm, alkaline springs catalysed the beginning of life [78]. The biodiverse and biological activity in hot springs may induce extremely high carbon isotopic fractionation in the hydrothermal sedimentary environment. The  $\delta^{13}\text{C}$  value of  $\text{CO}_2$  in the atmosphere has an average value of  $-7.7\%$  but varies seasonally and regionally. As a result of the biological activity, the  $\delta^{13}\text{C}$  value of marine carbonate formation has an average value of  $0\%$  [79]. Strong anaerobic fertilization may have occurred during the Mg-rich sedimentation process [80]. This carbon isotopic fractionation between the dissolved atmospheric carbon and magnesite also exists in the Hirsizdere and Bela Stena magnesite deposits [20,24,26], but it is high in the Kamado deposit. Therefore, the carbon sources for banded and massive magnesite ores in the Kamado deposit are best explained by a mixture of atmospheric  $\text{CO}_2$  and dissolved marine carbonates, which is similar to that of the magnesium source.

The  $\delta^{18}\text{O}_{\text{V-SMOW}}$  value ( $+22.8 \pm 0.7\%$  to  $23.0 \pm 1.0\%$ ; Table 2) of the banded magnesite ore increased compared to that of the stockwork magnesite ore, which was consistent with the  $\delta^{18}\text{O}_{\text{V-SMOW}}$  value ( $+21.6\%$  to  $+26.1\%$ ) of the Hirsizdere deposit (Turkey). The unusually low oxygen isotope ratio ( $\sim 25\%$ ) could be explained by depositional temperatures at or close to the boiling point [26]. The Kamado deposit was formed on the modern Tibetan Plateau, so the  $\delta^{18}\text{O}_{\text{V-SMOW}}$  value was relatively lower. The slightly lighter carbon isotope composition ( $\delta^{13}\text{C}_{\text{V-PDB}} = +7.3 \pm 0.3\%$  to  $+7.7 \pm 0.7\%$ ) of massive ore may indicate a decline in anaerobic fermentation during hot spring activity. The massive ore had an extremely high  $\delta^{18}\text{O}_{\text{V-SMOW}}$  value, ranging from  $+27.1 \pm 0.4\%$  to  $+29.5 \pm 0.3\%$ , which was similar to that of the Bela Stena deposit (Serbia) ( $\delta^{18}\text{O}_{\text{V-SMOW}}$  value was  $+32.8 \pm 2.1\%$ ). The oxygen isotope thermometer estimated that its formation temperature ranged from  $26$  to  $36\text{ }^\circ\text{C}$ , which may have deposited magnesite ore in a low-temperature environment at the bottom of the alkaline lake [24]. Due to the occurrence of oxygen isotope fractionation during the dehydration and mineralization processes of magnesite, the above estimated values may have errors and are used only as qualitative references for the comparison of mineralization temperatures [81].

In summary, the carbon sources for the Kamado magnesite ores varied between near-surface epithermal systems and lake conditions. The carbon in the vein or stockwork magnesite ores was sourced from a mixture of oxidized organic carbon and dissolved marine carbonates, while the strata-bound magnesite ores were sourced from a mixture of atmospheric dissolved carbon in lake waters and dissolved marine carbonates.

### 5.3. Genesis of the Kamado Magnesite Deposit

Aqueous solutions of moderate temperature and low salinity carrying  $\text{CO}_2$  may have affected the ultramafic rock by hydration and carbonation reactions. This progress may not be limited to the ultramafic rock mass but would also induce hydrothermal magnesium-rich carbonate sediments in lacustrine environments. Like the (hydro)magnesite deposits in the western Tethyan ophiolite suture zone, the Kamado, and Dujiali may represent their

constituents in the east. Massive strata-bound hydromagnesite stromatolites comprising cyanobacteria and diatoms in Salda Gölü and their diagenetically equivalent magnesite bodies in Hirsizdere were found to have developed in sediments in the Buyuk Mendere graben [82–84], an enclosed lacustrine basins above Mesozoic Yesilova ultramafic rocks in the Tethyan ophiolite suture [27]. Under the control of the volcanic activity caused by the rift, which formed under extensional stress since the Oligocene, the hot springs (13 °C to 36 °C) [68,85] caused by neotectonic activity brought magnesium from Yesilova ultramafic rocks that upwelled, forming the Salda Gölü hydromagnesite deposit in Salda Lake. The dehydration of early-stage hydromagnesite formed the Hirsizdere magnesite deposit. The pattern of hot springs supplying magnesian lacustrine sedimentation has also been observed in Bela Stena Lake (Serbia) near the Mirdita ophiolites [21,24]. Furthermore, this progress may also have occurred in the Bangong-Nujiang suture zone of the Tibetan Plateau. The Holocene hydromagnesite from Dujiali Lake exists in the sediments of the southwest Lunpola Basin [44,54,61,82,83], while the Kamado magnesite deposit is located southwest of the Nangqen strike-slip pull-apart basin. Both of them formed as strata-bound sediments near paleo-springs and ultrabasic rocks of the Bangong-Nujiang suture [41,42].

Associated with lateral extrusion that was induced by the India-Asia collision [86], the regional extensional stress in the Kamado area of the northeastern Tibetan Plateau during the early and middle Miocene resulted in a few pull-apart basins and composite back-arc and foreland basins [87], which may have induced geothermal activity [88]. Meteoric water gravitated down normal faults to be heated at depth by crustal heat and igneous intrusions. At the same time, CO<sub>2</sub> generated by thermal decarboxylation of organic-rich sediments mixed with hot waters contained a small component of abiogenically produced CO<sub>2</sub>. Aqueous solutions of moderate temperature and low salinity carrying CO<sub>2</sub> interacted with the ultramafic and carbonate country rocks via hydration and carbonation reactions. The fluids in the fractures were variously boiling, self-sealing, and eruptive. Mixing with meteoric water may have occurred close to the surface [89,90]. Magnesium was dissolved with bicarbonate, leaving silica behind, since silica is relatively insoluble in solutions rich in CO<sub>2</sub> [90]. Most of the iron and silica derived from the decomposition of the country rocks were carried towards the surface to form siliceous sinters, while magnesium carbonate or hydrous carbonate was precipitated nearly in situ as vein or stockwork ores (Figure 7). Iron may also have been precipitated as siderite or even as chromite or haematite.

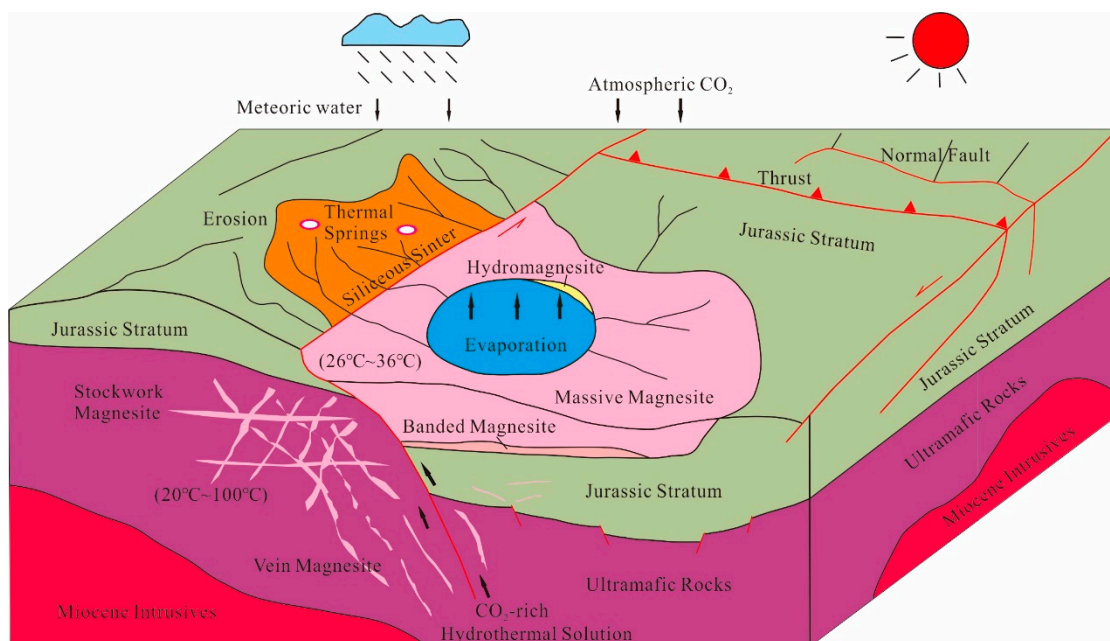


**Figure 7.** Genetic model of the Kamado magnesite deposit (modified from [24,28]).

## 6. Conclusions

The strata-bound orebody of Kamado may be the product of hot spring precipitation in the evaporative environment of alkaline lakes on the Tibetan Plateau, with its metallogenic mechanism similar to that of the lacustrine magnesite deposits of Bela Stena (Serbia) and Hirsizdere (Turkey) on the western edge of the Tethys belt. The ore-forming magnesium elements of the strata-bound ore body of the Kamado may come from the metasomatism and leaching of the ultramafic rocks by the circulating groundwater, while the carbon elements may mainly come from the alkaline lake, which dissolved atmospheric carbon dioxide and carbon dioxide from anaerobic fermentation during deposition.

**Author Contributions:** Original draft, X.Y.; Review & editing, G.H.; Project administration, Y.C., D.W. and F.H.; Data curation, Y.X.; Investigation, H.C., S.Y., H.L., L.H. and Y.L. All authors have read and agreed to the published version of the manuscript.

**Funding:** This research was funded by the China Geological Survey (grant numbers: DD20190379, DD20221695, and DD20190167), the China Scholarship Council (grant number: 201808110080), and the Institute of Mineral Resources, Chinese Academy of Geological Science Research Fund (grant number: kk2002).

**Data Availability Statement:** Data are contained within the article.

**Acknowledgments:** Thanks to the three reviewers and colleagues who put forward valuable suggestions for the article.

**Conflicts of Interest:** The authors declare no conflict of interest.

## References

- Drnek, T.L.; Moraes, M.N.; Neto, P.B. Overview of magnesite. *J. Refractory Innov. RHIM Bull.* **2018**, *1*, 14–22.
- Redlich, K.A. Die Typen der Magnesitlagerstätten. *Z. Prakt. Geol.* **1909**, *17*, 300–310.
- Nishihara, H. Origin of the bedded magnesites of Manchuria. *Econ. Geol.* **1956**, *51*, 698–711. [[CrossRef](#)]
- Zhang, Q.S. Early proterozoic tectonic styles and associated mineral deposits of the North China platform. *Precambrian Res.* **1988**, *39*, 1–29. [[CrossRef](#)]
- Melezhik, V.A.; Fallick, A.E.; Medvedev, P.V.; Makarikhin, V.V. Palaeoproterozoic magnesite: Lithological and isotopic evidence for playa/sabkha environments. *Sedimentology* **2001**, *48*, 379–397. [[CrossRef](#)]
- Jiang, S.Y.; Chen, C.X.; Chen, Y.Q.; Jiang, Y.H.; Dai, B.Z.; Ni, P. Geochemistry and genetic model for the giant magnesite deposits in the eastern Liaoning Province, China. *Acta Petrol. Sin.* **2004**, *20*, 765–772.
- Power, I.M.; Wilson, S.A.; Harrison, A.L.; Dipple, G.M.; Mccutcheon, J.; Southam, G.; Kenward, P.A. A depositional model for hydromagnesite-magnesite playas near Atlin, British Columbia, Canada. *Sedimentology* **2014**, *61*, 1701–1733. [[CrossRef](#)]
- Dong, A.G.; Zhu, X.K.; Li, S.Z.; Kendall, B.; Wang, Y.; Gao, Z.F. Genesis of a giant Paleoproterozoic strata-bound magnesite deposit: Constrains from Mg isotopes. *Precambrian Res.* **2016**, *281*, 673–683. [[CrossRef](#)]
- Velasco, F.Q.; Pesquera, A.; Arce, R.; Olmedo, F. A contribution to the ore genesis of the magnesite deposit of Eugui, Navarra (Spain). *Miner. Depos.* **1987**, *22*, 33–41. [[CrossRef](#)]
- Aharon, P. A stable-isotope study of magnesites from the Rum Jungle uranium field, Australia: Implications for the origin of strata-bound massive magnesites. *Chem. Geol.* **1988**, *69*, 127–145. [[CrossRef](#)]
- Joshi, P.; Pant, P.D.; Upadhyaya, R.C. Petrography and geochemistry of magnesite and talc deposits of Jhiroli, Kumaun Lesser Himalaya. In *Magmatism, Tectonism and Mineralization*; Macmillan Publishers India Ltd.: New Delhi, India, 2009; pp. 215–229.
- Barnes, I.; O’Neil, J.R.; Trescases, J.J. Present day serpentinization in New Caledonia, Oman and Yugoslavia. *Geochim. Cosmochim. Acta* **1978**, *42*, 144–145. [[CrossRef](#)]
- Abu-Jaber, N.S.; Kimberley, M.M. Origin of ultramafic-hosted vein magnesite deposits. *Ore Geol. Rev.* **1992**, *7*, 155–191. [[CrossRef](#)]
- Alcicek, H. Late Miocene nanmarine sedimentation and formation of magnesites in the Acigol Basin, southwestern Anatolia, Turkey. *Sediment. Geol.* **2009**, *219*, 115–135. [[CrossRef](#)]
- Oskierski, H.C.; Bailey, J.G.; Kennedy, E.M.; Jacobsen, G.; Ashley, P.M.; Dlugogorski, B.Z. Formation of weathering-derived magnesite deposits in the New England Orogen, New South Wales, Australia: Implications from mineralogy, geochemistry and genesis of the Attunga magnesite deposit. *Miner. Depos.* **2013**, *48*, 525–541. [[CrossRef](#)]
- Oskierski, H.C.; Dlugogorski, B.Z.; Jacobsen, G. Sequestration of atmospheric CO<sub>2</sub> in a weathering-derived, serpentinite-hosted magnesite deposit: 14C tracing of carbon sources and age constraints for a refined genetic model. *Geochim. Cosmochim. Acta* **2013**, *122*, 226–246. [[CrossRef](#)]
- Oskierski, H.C.; Beinlich, A.; Mavromatis, V.; Altarawneh, M.; Dlugogorski, B.Z. Mg isotope fractionation during continental weathering and low temperature carbonation of ultramafic rocks. *Geochim. Cosmochim. Acta* **2019**, *262*, 60–77. [[CrossRef](#)]

18. Rielli, A.; Boschi, C.; Dini, A. Tectonically driven carbonation of serpentinite by mantle CO<sub>2</sub>: Genesis of Castiglioncello magnesite deposit in the Ligurian ophiolite of central Tuscany (Italy). *Ore Geol. Rev.* **2022**, *149*, 105022. [[CrossRef](#)]
19. Pohl, W.; Siegl, W. Sediment-hosted magnesite deposits. In *Handbook of Strata-Bound and Stratiform Ore Deposits*; Wolf, K.H., Ed.; Elsevier: Amsterdam, The Netherlands, 1986; Volume 14, pp. 223–310.
20. Kralik, M.; Aharon, P.; Zachmann, D.W. Carbon and oxygen isotope systematics of magnesites: A review. *Monograph Ser. Miner. Depos.* **1989**, *28*, 197–223.
21. Beinlich, A.; Austrheim, H. In situ sequestration of atmospheric CO<sub>2</sub> at low temperature and surface cracking of serpentinized peridotite in mine shafts. *Chem. Geol.* **2012**, *332–333*, 32–44. [[CrossRef](#)]
22. Boschi, C.; Dini, A.; Dallai, L.; Ruggieri, G.; Gianelli, G. Enhanced CO<sub>2</sub>-mineral sequestration by cyclic hydraulic fracturing and Si-rich fluid infiltration into serpentinites at Malentrata (Tuscany, Italy). *Chem. Geol.* **2009**, *265*, 209–226. [[CrossRef](#)]
23. De Deckker, P. Groundwater interactions control dolomite and magnesite precipitation in saline playas in the Western District Volcanic Plains of Victoria, Australia. *Sediment. Geol.* **2019**, *380*, 105–126. [[CrossRef](#)]
24. Fallick, A.E.; Ilich, M.; Russell, M.J. A stable isotope study of the magnesite deposits associated with the Alpine-type ultramafic rocks of Yugoslavia. *Econ. Geol.* **1991**, *86*, 847–861. [[CrossRef](#)]
25. Russell, M.J. The generation at hot spring of sedimentary ore deposits, microbialites and life. *Ore Geol. Rev.* **1996**, *10*, 199–214. [[CrossRef](#)]
26. Zedef, V.; Russell, M.J.; Fallick, A.E.; Hall, A.J. Genesis of vein stockwork and sedimentary magnesite and hydromagnesite deposits in the ultramafic terranes of southwestern Turkey: A stable isotope study. *Econ. Geol.* **2000**, *95*, 429–445. [[CrossRef](#)]
27. Schroll, E. Genesis of magnesite deposits in the view of isotope geochemistry. *Bol. Parana. Geociências* **2002**, *50*, 59–68. [[CrossRef](#)]
28. Pohl, W. Genesis of magnesite deposits—Models and trends. *Geol. Rundsch.* **1990**, *79*, 291–299. [[CrossRef](#)]
29. del Real, P.G.; Maher, K.; Kluge, T.; Bird, D.K.; Brown, G.E., Jr.; John, C.M. Clumped-isotope thermometry of magnesium carbonates in ultramafic rocks. *Geochim. Cosmochim. Acta* **2016**, *193*, 222–250. [[CrossRef](#)]
30. Falk, E.S.; Kelemen, P.B. Geochemistry and petrology of listvenite in the Samail ophiolite, Sultanate of Oman: Complete carbonation of peridotite during ophiolite emplacement. *Geochim. Cosmochim. Acta* **2015**, *160*, 70–90. [[CrossRef](#)]
31. Bucher, K.; Grapes, R. Metamorphism of Ultramafic Rocks. In *Petrogenesis of Metamorphic Rocks*; Springer: Berlin/Heidelberg, Germany, 2023; pp. 209–247.
32. Chen, Y.C.; Wang, D.H.; Xu, Z.G. *Important Minerals and Regional Metallogenic Regularity in China*; Geological Publishing House: Beijing, China, 2015. (In Chinese)
33. Song, Y.; Zeng, Q.G.; Liu, H.Y.; Liu, Z.B.; Li, H.F.; Dexi, Y.Z. An innovative perspective for the evolution of Bangong-Nujiang Ocean: Also discussing the Paleo- and Neo-Tethys conversion. *Acta Petrol. Sin.* **2019**, *35*, 625–641. (In Chinese with English Abstract)
34. Ding, J.H.; Chen, Z.H.; Yang, G.J.; Deng, F.; Lou, D.B. Metallogeny and resource potential of magnesite deposits in China. *Geol. China* **2013**, *40*, 1699–1711. (In Chinese with English Abstract)
35. Zhao, Z.; Bai, G.; Wang, D.H.; Chen, Y.C.; Xu, Z.G. The Metallogenic Belts of Chinese Magnesite Deposits and Key Scientific Issues. *Acta Geol. Sin.* **2014**, *88*, 2326–2338. (In Chinese with English Abstract)
36. Ilich, M. *Hydrothermal-Sedimentary Magnesite Deposit of Neovade, Gornji Milanovac (Western Serbia)*: Zbornik Radova Rudarsko-Geoloskog Fakulteta; University of Beograd, Faculty of Mining and Geology Transactions: Belgrade, Serbia, 1976; Volume 19, pp. 307–329.
37. Dilek, Y.; Furnes, H. Structure and geochemistry of Tethyan ophiolites and their petrogenesis in subduction rollback systems. *Lithos* **2009**, *113*, 1–20. [[CrossRef](#)]
38. Wu, F.Y.; Wan, B.; Zhao, L.; Xiao, W.J.; Zhu, R.X. Tethyan geodynamics. *Acta Petrol. Sin.* **2020**, *36*, 1627–1674. (In Chinese with English Abstract)
39. Zhu, R.X.; Zhao, P.; Zhao, L. Tectonic evolution and geodynamics of the Neo-Tethys Ocean. *Sci. China Earth. Sci.* **2022**, *65*, 1–24. (In Chinese with English Abstract) [[CrossRef](#)]
40. Yin, A.; Harrison, T.M. Geologic evolution of the Himalayan-Tibetan orogen. *Annu. Rev. Earth Planet. Sci.* **2000**, *28*, 211–280. [[CrossRef](#)]
41. Xiong, F.H.; Yang, J.S.; Dilek, Y.; Xu, X.Z.; Zhang, Z.M. Origin and significance of diamonds and other exotic minerals in the Dingqing ophiolite peridotites, eastern Bangong-Nujiang suture zone, Tibet. *Lithosphere* **2017**, *10*, 142–155. [[CrossRef](#)]
42. Liu, F.; Yang, J.S.; Lian, D.Y.; Li, G.L. Geological features of Neothyan ophiolites in Tibetan Plateau and its tectonic evolution. *Acta Petrol. Sin.* **2020**, *36*, 2913–2945. (In Chinese with English Abstract)
43. Tapponnier, P.; Xu, Z.Q.; Roger, F.; Meyer, B.; Arnaud, N.; Wittlinger, G.; Yang, J.S. Oblique stepwise rise and growth of the Tibet Plateau. *Science* **2001**, *294*, 1671–1677. [[CrossRef](#)]
44. Zheng, M.P.; Xiang, J.; Wei, X.J.; Zheng, Y. *Saline Lakes on the Qinghai-Xizang(Tibet) Plateau*; Beijing Science and Technology Press: Beijing, China, 1989; pp. 1–431. (In Chinese with English Abstract)
45. Zhang, W.; Tan, H.; Xu, W.; Huang, J. Boron source and evolution of the Zabuye salt lake, Tibet: Indication from boron geochemistry and isotope. *Appl. Geochem.* **2023**, *148*, 105516. [[CrossRef](#)]
46. Eleng, H.I.; Tan, H.B.; Su, J.B.; Yang, J.Y. Origin of the enrichment of B and alkali metal elements in the geothermal water in the Tibetan Plateau: Evidence from B and Sr isotopes. *Geochemistry* **2021**, *81*, 125797. [[CrossRef](#)]
47. Tan, H.B.; Shi, Z.W.; Cong, P.X.; Xue, F.; Chen, G.H. The spatial distribution law of B, Li, Rb and Cs elements and supernormal enrichment mechanism in Tibet geothermal system. *Sediment. Geol. Tethyan Geol.* **2023**, *43*, 404–415.

48. Tang, Y.; Zhai, Q.G.; Chung, S.L.; Hu, P.Y.; Wang, J.; Xiao, X.C.; Song, B.; Wang, H.T.; Lee, H.Y. First mid-ocean ridge-type ophiolite from the Meso-Tethys suture zone in the north-central Tibetan plateau. *Geol. Soc. Am. Bull.* **2020**, *132*, 2202–2220. [[CrossRef](#)]
49. Jiang, S.; Jiang, Y.; Liu, Y.; Li, S.; Zhang, W.; Wang, G.; Lu, L.; Somerville, I. The Bangong-Nujiang Suture Zone, Tibet Plateau: Its role in the tectonic evolution of the eastern Tethys Ocean. *Earth-Sci. Rev.* **2021**, *218*, 103656. [[CrossRef](#)]
50. Zheng, X.Y.; Zhang, M.G.; Xu, X.; Li, B.X. *Saline Lakes of China*; Science Press: Beijing, China, 2002; pp. 1–415. (In Chinese)
51. O'Neil, J.R. Stable isotopes in mineralogy. *Phys. Chem. Miner.* **1977**, *2*, 105–123. [[CrossRef](#)]
52. Das Sharma, S.; Patil, D.J.; Gopalan, K. Temperature dependence of oxygen isotope fractionation of CO<sub>2</sub> from magnesite-phosphoric acid reaction. *Geochim. Cosmochim. Acta* **2002**, *66*, 589–593. [[CrossRef](#)]
53. Kim, S.-T.; Coplen, T.B.; Horita, J. Normalization of stable isotope data for carbonate minerals: Implementation of IUPAC guidelines. *Geochim. Cosmochim. Acta* **2015**, *158*, 276–289. [[CrossRef](#)]
54. Lin, Y.J.; Zheng, M.P.; Ye, C.Y. Hydromagnesite precipitation in the Alkaline Lake Dujiali, central Qinghai-Tibetan Plateau: Constraints on hydromagnesite precipitation from hydrochemistry and stable isotopes. *Appl. Geochem.* **2017**, *78*, 139–148. [[CrossRef](#)]
55. Jurković, I.; Palinkaš, L.A.; Garašić, V.; Strmić Palinkaš, S. Genesis of vein-stockwork cryptocrystalline magnesite from the Dinaride ophiolites. *Ofoliti* **2012**, *37*, 13–26.
56. Hoke, L.; Lamb, S.; Hilton, D.R.; Poreda, R.L. Southern limit of mantle-derived geothermal helium emissions in Tibet: Implications for lithospheric structure. *Earth Planet. Sci. Lett.* **2000**, *180*, 297–308. [[CrossRef](#)]
57. Hou, Z.Q.; Li, Z.Q. Possible location for underthrusting front of the Indus continent: Constraints from Helium isotope of the geothermal gas in the southern Tibet and eastern Tibet. *Acta Geol. Sin.* **2004**, *78*, 382–393. (In Chinese with English Abstract)
58. Klemperer, S.L.; Zhao, P.; Shi, D.N.; Crossey, L.J.; Karlstrom, K.E.; Winn, C.L.; Liu, T.Z.; Xiong, Z.Y.; Guo, X.D.; Zeng, D.; et al. Detection of a widespread mantle component of <sup>3</sup>He in thermal springs of Lhasa Block and Tethyan Himalaya, eastern Tibet: Evidence for roll-back of the Indian-Asian mantle suture. In Proceedings of the International Symposium on Deep Earth Exploration and Practices, Beijing, China, 24–26 October 2018.
59. Su, J.B.; Tan, H.B.; Chen, X. The groundwater deep circulation and large-scale geothermal deposition in response to the extension of the Yadong-Gulu rift, South Tibet, China. *J. Volcanol. Geotherm. Res.* **2020**, *395*, 106836. [[CrossRef](#)]
60. Wang, S.Q.; Lu, C.; Nan, D.W.; Hu, X.C.; Shao, J.L. Geothermal resources in Tibet of China: Current status and prospective development. *Environ. Earth Sci.* **2017**, *76*, 239. [[CrossRef](#)]
61. Lin, Y.J.; Zheng, M.P.; Ye, C.Y.; Power, I.M. Trace and rare earth element geochemistry of Holocene hydromagnesite from Dujiali Lake, central Qinghai-Tibetan Plateau, China. *Carbonates Evaporites* **2017**, *3–4*, 1–15. [[CrossRef](#)]
62. Ji, C.; Zhang, K.J.; Yan, L.L. Hydrothermal metasomatism and solid-phase transfer in petrogenesis of listvenite: The Meso-Tethyan ophiolite, central Tibet, China. *Contrib. Mineral. Petrol.* **2023**, *178*, 4. [[CrossRef](#)]
63. Hannigan, R.E. Rare earth, major and trace elements geochemistry of surface and geothermal waters from the Tanpo volcanic zone, north island New Zealand. *Rare Earth Elem. Groundw. Flow Syst.* **2005**, *51*, 67–88.
64. Wang, M.M.; Zhou, X.; Liu, Y.; Xu, H.F.; Wu, Y.Q.; Zhuo, L.Y. Major, trace and rare earth elements geochemistry of geothermal waters from the Rehai high-temperature geothermal field in Tengchong of China. *Appl. Geochem.* **2020**, *119*, 1–12. [[CrossRef](#)]
65. Chudaev, O.V.; Chelnokov, G.A.; Bragin, I.V.; Kharitonova, N.A.; Rychagov, S.N.; Nuzhdaev, A.A.; Nuzhdaev, I.A. Rare earth and major elements geochemistry of geothermal waters from Mutnovsky Volcano, Kamchatka. *Procedia Earth Planet. Sci.* **2017**, *17*, 92–95. [[CrossRef](#)]
66. Morteani, G.; Moeller, P.; Schley, F. The rare earth element contents and the origin of the sparry magnesite mineralizations of Tux-Lanersbach, Entachen Alm, Spiessnaegel, and Hochfilzen, Austria, and the lacustrine magnesite deposits of Aiani-Kozani, Greece, and Bela Stena, Yugoslavia. *Econ. Geol.* **1982**, *77*, 617–631. [[CrossRef](#)]
67. Morteani, G.; Schley, F.; Moller, P. On the formation of magnesite. In *Mineral Deposits of the Alpine Epoch in Europe*; Schneider, H.J., Ed.; Springer: Berlin/Heidelberg, Germany, 1983; pp. 237–266.
68. Braithwaite, C.J.R.; Zedef, V. Hydromagnesite stromatolites and sediments in an alkaline lake, Salda Golu, Turkey. *J. Sediment. Res.* **1996**, *66*, 991–1002.
69. Zedef, V. The Origin of Magnesite in Turkey, a Stable Isotope Study. Unpublished. Ph.D. Thesis, Glasgow University, Glasgow, UK, 1994.
70. Veizer, J.; Hoefs, J. The nature of <sup>18</sup>O/<sup>16</sup>O and <sup>13</sup>C/<sup>12</sup>C secular trends in sedimentary carbonate rocks. *Geochim. Cosmochim. Acta* **1976**, *40*, 1387–1395. [[CrossRef](#)]
71. Falk, E.S.; Guo, W.; Paukert, A.N.; Matter, J.M.; Mervine, E.M.; Kelemen, P.B. Controls on the stable isotope compositions of travertine from hyperalkaline springs in Oman: Insights from clumped isotope measurements. *Geochim. Cosmochim. Acta* **2016**, *192*, 1–28. [[CrossRef](#)]
72. Bekker, A.; Karhu, J.A.; Eriksson, K.A.; Kaufman, A.J. Chemostratigraphy of Paleoproterozoic carbonate successions of the Wyoming Craton: Tectonic forcing of biogeochemical change? *Precambrian Res.* **2003**, *120*, 279–325. [[CrossRef](#)]
73. Bekker, A.; Eriksson, K.A. A Paleoproterozoic drowned carbonate platform on the southeastern margin of the Wyoming Craton: A record of the Kenorland breakup. *Precambrian Res.* **2003**, *120*, 327–364. [[CrossRef](#)]
74. Bekker, A.; Karhu, J.A.; Kaufman, A.J. Carbon isotope record for the onset of the Lomagundi carbon isotope excursion in the Great Lakes area, North America. *Precambrian Res.* **2006**, *148*, 145–180. [[CrossRef](#)]

75. Schidlowski, M.; Eichmann, R.; Junge, C.E. Carbon isotope geochemistry of the Precambrian Lomagundi carbonate province, Rhodesia. *Geochim. Cosmochim. Acta* **1976**, *40*, 449–455. [[CrossRef](#)]
76. Karhu, J.A.; Holland, H.D. Carbon isotopes and the rise of atmospheric oxygen. *Geology* **1996**, *24*, 867–870. [[CrossRef](#)]
77. Tang, H.S.; Chen, Y.J.; Santosh, M.; Zhong, H.; Wu, G.; Lai, Y. C–O isotope geochemistry of the Dashiqiao magnesite belt, North China Craton: Implications for the Great Oxidation Event and ore genesis. *Geol. J.* **2013**, *48*, 467–483. [[CrossRef](#)]
78. Russell, M.J.; Hall, A.J. The onset and early evolution of life. In *Evolution of Early Earth's Atmosphere, Hydrosphere, and Biosphere—Constraints from Ore Deposits: Geological Society of America Memoir*; Kesler, S.E., Ohmoto, H., Eds.; Geological Society of America location: Boulder, CO, USA, 2006; Volume 198, pp. 1–32.
79. Hoefs, J. Isotope fractionation processes of selected elements. In *Stable Isotope Geochemistry*; Springer: Cham, Switzerland, 2021; pp. 58–63.
80. Irwin, H.; Curtis, C.; Coleman, M.L. Isotopic evidence for source of diagenetic carbonates formed during burial of organic-rich sediments. *Nature* **1977**, *269*, 209–213. [[CrossRef](#)]
81. Wenner, D.B.; Taylor, H.P. Oxygen and hydrogen isotope studies of the serpentinization of ultramafic rocks in oceanic environments and continental ophiolite complexes. *Am. J. Sci.* **1973**, *273*, 207–239. [[CrossRef](#)]
82. Lin, Y.J.; Zheng, M.P.; Ye, C.Y.; Power, I.M. Rare earth element and strontium isotope geochemistry in Dujiali Lake, central Qinghai-Tibet Plateau, China: Implications for the origin of hydromagnesite deposits. *Geochemistry* **2019**, *79*, 337–346. [[CrossRef](#)]
83. Zheng, M.P.; Zhang, Y.S.; Liu, X.F.; Nie, Z.; Kong, F.J.; Qi, W.; Jia, Q.X.; Pu, L.Z.; Hou, X.H.; Wang, H.L.; et al. Progress and Prospects of Salt Lake Research in China. *Acta Geol. Sin.-Engl.* **2016**, *90*, 1195–1235. [[CrossRef](#)]
84. Koçyigit, A. Güneybatı Tütkiye ve yakın dolayında levha içi yeni tektonik gelişim. *Geol. Soc. Turk. Bull.* **1984**, *27*, 1–16.
85. Braithwaite, C.J.R.; Zedef, V. Living hydromagnesite stromatolites from Turkey. *Sediment. Geol.* **1994**, *92*, 1–5. [[CrossRef](#)]
86. Tapponnier, P.; Molnar, P. Slip-line field theory and large-scale continental tectonics. *Nature* **1976**, *264*, 319–324. [[CrossRef](#)]
87. Qin, X.W.; Ma, H.Z.; Zhang, X.Y.; Hu, X.S.; Li, G.R.; Cheng, H.D.; Han, J.B.; Li, Y.S.; Miao, W.L.; Han, W.H.; et al. Origin and Circulation of Springs in the Nangqen and Qamdo Basins, Southwestern China, Based on Hydrochemistry and Environmental Isotopes. *Geofluids* **2022**, *2022*, 7190994. [[CrossRef](#)]
88. Zhu, J.L.; Hu, K.Y.; Lu, X.L.; Huang, X.X.; Liu, K.T.; Wu, X.J. A Review of Geothermal Energy Resources, Development, and Applications in China: Current Status and Prospects. *Energy* **2015**, *93*, 466–483. [[CrossRef](#)]
89. Nelson, C.E.; Giles, D.L. Hydrothermal eruption mechanisms and hot spring gold deposits. *Econ. Geol.* **1985**, *80*, 1633–1639. [[CrossRef](#)]
90. Shettel, D.L. Solubility of quartz in H<sub>2</sub>O-CO<sub>2</sub> fluids at 5 kb and 500–900 C. *Am. Geophys. Union Trans.* **1973**, *54*, 480.

**Disclaimer/Publisher's Note:** The statements, opinions and data contained in all publications are solely those of the individual author(s) and contributor(s) and not of MDPI and/or the editor(s). MDPI and/or the editor(s) disclaim responsibility for any injury to people or property resulting from any ideas, methods, instructions or products referred to in the content.